International Journal of Computational Intelligence Research
ISSN 0973-1873 Volume 13, Number 5 (2017), pp. 1307-1331

http://www.ripublication.com

Iris Recognition System based on ZM, GF, VR and Matching Level Fusion

GanapathiV. Sagar[1], K B Raja[2], K Suresh Babu[2], Chetan Tippanna Madiwalar[2] and Venugopal K R[2]

[1]Dr. Ambedkar Institute of Technology, Bangalore, India.

[2]University Visveswaraya Collage of Engineering, Bangalore University, Bangalore, India

Abstract

Isis is the physiological biometric trait used to recognized a person efficiently. In this paper, we propose Iris Recognition System based on ZM, GF, VR and Matching Level Fusion. The Region of Interest (ROI) of iris is extracted using segmentation. Zernike Moments (ZM) is applied on segmented iris images to extract ZM features. The novel concept of many feature vectors of a single person are converted into single vector per person ie., Vectors Reduction (VR). The Euclidian Distance (ED) is used to compare feature vectors in the database with feature vectors in test section to compute the performance parameters. The Gabor Filter (GF) is also used to extract features of iris. Many GF feature vectors of single person are connected into single feature vector per person. The ED is used to compare database and test feature vectors to compute performance parameters. The performance parameters obtained from ZM and GF are fused using normalization technique to improve the performance parameters. It is observed that, the performance parameters are better compared to existing techniques.

Keywords: Biometrics, Iris Recognition, Zernike Moments, Gabor Filter, Matching Level Fusion.

1. INTRODUCTION:

The biometrics are used to authenticate persons effectively compared to traditional methods of reorganization using Personal Identification (PID), smart cards etc. Biometrics refers to a science of analyzing human body parts for security purposes. Biometric technologies are becoming the foundation of an extensive array of highly secure identification and personal verification solutions. As the level of security

breaches and transaction fraud increases, the need for highly secure identification and personal verification technologies are becoming apparent. The disadvantages of traditional methods are recall of PIN is difficult; the smart cards may be lost or stolen. The advantages of biometrics traits are the parts of human body and behavior of humans; hence limitation of traditional methods are eliminated. The biometric trades are broadly classified into two groups' viz., (i) physiological traits and (ii) behavioral traits. The physiological traits are body parts such as fingerprints, palm prints, Iris, Face etc., which are almost constant throughout the life time of a person. The behavioral traits are related to the behavior of person such as gait, signature, key stroke etc., which vary in accordance with circumstances.

Contribution: In this paper, iris recognition system is developed based on ZM and GF features. The number of iris feature vectors of single person are converted into single iris feature. The performance parameters are computed using ZM and GF separately. The performance parameters obtained from ZM and GF are fused to improve performance of the biometric system.

Organization: The remaining sections of this paper are structured as follows. Section 2 explains the literature survey of existing techniques. Section 3 describes the proposed iris recognition model. The performance analysis is discussed in section 4. Conclusion is given in Section 5.

2. LITERATURE SURVEY:

Mohammed A. M et al, [1] proposed a novel segmentation method for non-ideal iris images. Since the performance in non-ideal iris images is influenced by the segmentation accuracy of an iris recognition system, this includes pupil segmentation and iris visible and NIR light for pupil segmentation. The active counter is initialized near the desired object boundary to reduce the execution time and to achieve robust segmentation. For iris segmentation, the line Hough transforms were employed for eyelid detection. Hence if the eyelid is closed, the counter will shrink and if eyelid is open, the counter will expand from the initial mask. John Daugman and Cathryn Downing, [2] proposed standard iris images are 600 times larger than the iris code templates computed from them for database storage and search. If it is desired that iris data should be stored, transmitted and embedded in media in the form of images. To achieve this aim with its implications for bandwidth storage. The proposed scheme is that to combine region of interest isolation with Jpeg and Jpeg 2000 compression at severe levels and these are tested using a publically available database of iris images. This also shows that only about 2% to 3% of the iris code bits change as a consequence of image compression even as severe as to 2000 bytes. The entropy associated with states of bits in iris codes calculated from different images of the same eye, is typically 0.506 bits. Pattabhi Ramaiah Nalla and Ajay Kumar, [3] proposed a domain adaptation frame work because the performance degradation is possible while matching iris images which are acquired under two different domains. A new algorithm is introduced using markov random field's model to significantly improve cross-domain iris recognition. The iris recognition accuracy is improved by acquiring

Iris images invisible and near infrared light. The performance improvement for the cross-spectral Iris recognition is significantly higher as compared to the cross sensor Iris recognition. Mohd Tarif khan et al, [4] proposed Iris recognition system using 1D Gabor filter to extract the unique features which include real and imaginary parts by using 1D normalization and segmenting the Iris and pupil boundaries of eye from database images. The Center boundaries are quickly detected even in the presence of eye lashes, noise and excess illumination. The excellent accuracy with excellent processing speed is resulted by testing different Iris databases with noisy images and noise free images. Hamming distance based matching algorithm is used for iris template matching because it shows excellent processing speed. Chun-wei tan and Ajay Kumar, [5] proposed an efficient Iris segmentation approach for segmenting Iris images acquired from at a distance less constrained imaging conditions. The Iris segmentation approach is designed based on the cellular automata which evolves using the Grow-Cut algorithm. The method achieved average improvement of 34.8%, 31.5%and 31.4% in the average segmentation error which was obtained from the three publicly available databases. The result of on algorithm illustrates the significant reduction in complexity of Iris segmentation which reduces significantly the computational cost.

Hau Ngo et al, [6] proposed a hardware design for a real time Iris segmentation system based on an FPGA device. The iris image is detected by using the canny edge detection algorithm and circle search. The parallel architecture which utilizes embedded memory bits to retain binary images and reduce communication with external memory chip. Memory controller will distribute the internal memory to keep access time low and simulation results shows great speedup achieved by the parallel architecture method compared CPU based implementation. Vaibhav. V.Dakre Pravin, [7] proposed multi-model biometrics based on combination of face and iris biometric features. In an image, face is detected using Vi ola jones algorithms and these make use of circular Hough transform for iris segmentation. The images are pre-processed and segmented successfully. The feature vectors are fused at feature level fusion using z-norm technique and forming a single vector. Lydia Elizabath et al, [8] proposed a novel approach of grid based iris biometric water marking technique based on a canny edge detection algorithm. The grid based watermarking algorithm uses a hybrid Singular Value Decomposition (SV D) and Discrete Wavelet Transform (DWT). The hybrid DWT and SVD together makes the watermarking scheme strong and undetectable. In this scheme fault acceptance rate and fault error rate areminimized efficiently. Simina Emerich et al, [9] proposed iris feature extraction based on dense descriptors and also captures local details, pixel by pixel over the complete image. In order to capture both spatial and frequency information. The three different techniques are presented viz., Local Binary Pattern (LBP), Local Phase Quantization(LPQ) and Differential Excitation. The experiments were performed on the UPOL database, which are captured in the visible light due to clarity of the texture present in the component images. These suggest that rotation invariant LBP and rotation invariant LPQ descriptors are good for iris texture analysis. This results in the iris micro-texture patterns such as crypts, furrows or pigment spots which are characterized by patched based descriptors.

Diego Grangnaniello et al, [10] proposed a number of image descriptors for the live-ness detection task in authentication system based on various biometric traits such as face, iris and fingerprint. Both simple descriptors with independent quantization of features, already considered for some live-ness detection tasks and more complex ones, based on the joint quantization of rich features, have been considered. Hau T.Ngo et al, [11] presented an architecture design for a high performance iris boundary detection system based on FPGA. A novel design and implementation using circular Hough transform was proposed to reduce the memory requirement by 93% as compared to the direct implementation of the circular of transform while maintaining a high detection rate of 92%. The parallel pipeline implementation of the proposed architecture demonstrates a high speed processing capability to support real-time iris recognition system. Therefore, the proposed technology is used in portable consumer devices such as tablets and mobile phones where iris recognition algorithm is used. Sheng-Hsun Hsieh et al, [12] proposed a novel hardware-software hybrid method to increase the stand-off distance in an iris recognition system. The system hardware design used is optimized wavefront coding technique to extend the depth of field. By using wave front coding to compensate for the blurring of the image on the software side, the local patch-based super-resolution method to restore the blurred image to its clear version. The proposed system increases the capture volume of a conventional iris recognition system by three times and maintained the system high recognition rate. Raghavendra and Busch, [13] presents depth analysis of presentation attacks on iris recognition system especially focusing on the photo print attacks and the electronic display attack. The algorithm introduced relatively large scale visible spectrum iris artifact database consists of 3300 iris normal and artifact samples that are captured by simulating iris recognition system by using five different attacks. Multiscale binarized statistical image features and linear support vector machine are used based on Presentation Attack Detection (PAD). Extensive experiments are carried out on four different publically available iris artifact databases results outstanding performance of the PAD scheme with various well established state of the art schemes. Nadia Othman and Bernodette [14] proposed several novel contributions to the problem of iris performance decrease due to degradations of the iris image, occurring in particular when the acquisition distance is increased. The approach is based on simple SR techniques applied on four different frames of video to improve by taking into account some quality criteria such as (i) the super resolution improves significantly the performance of iris recognition only when the images are of good quality. This is the case, when the fusion involves, images are taken from short distances or the best images from long distances. ii] the local quality super resolution approach enhances the performance for the short distances, the quality of the image decreases and for the long distances, the quality of the image performances increases using local quality super resolution approach, bad segmented pixels are detected and to discard them from the fusion procedure by using local quality measure.

3. PROPOSED MODEL

In this section, we present the proposed iris recognition model based on ZM, GF, reduction of feature vectors and fusion at matching level. The iris template is created and features are extracted using ZM and GF. The numbers of features vectors of single persons are converted into single person are converted into single feature vector concept is introduced. The performance parameters are fused in matching level to enhanced results. The block diagram of the model is shown in figure 1.

3.1Iris database

A stable and unique internal organ of eye with rich texture features present between pupil and sclera boundary in eye. The eye images captured under Near Infrared light source provide better iris patterns with good contrast and illuminations. The Chinese Academy of Science Institute and Automation (CASIA) V.1 Iris database [15] created with NIR light source consists of 108 persons having each person's seven different images forming total 756 eye images. In the Iris database, the seventh image of every person is considered as test Iris image. The eye images of CASIA V.1 database of a single person is shown in figure.2. The Total Success Rate (TSR), False Rejection Rate (FRR) and False Accept Rate (FAR) are computed by considering number of Person inside Database (PID) and number of Persons outside Database (POD).

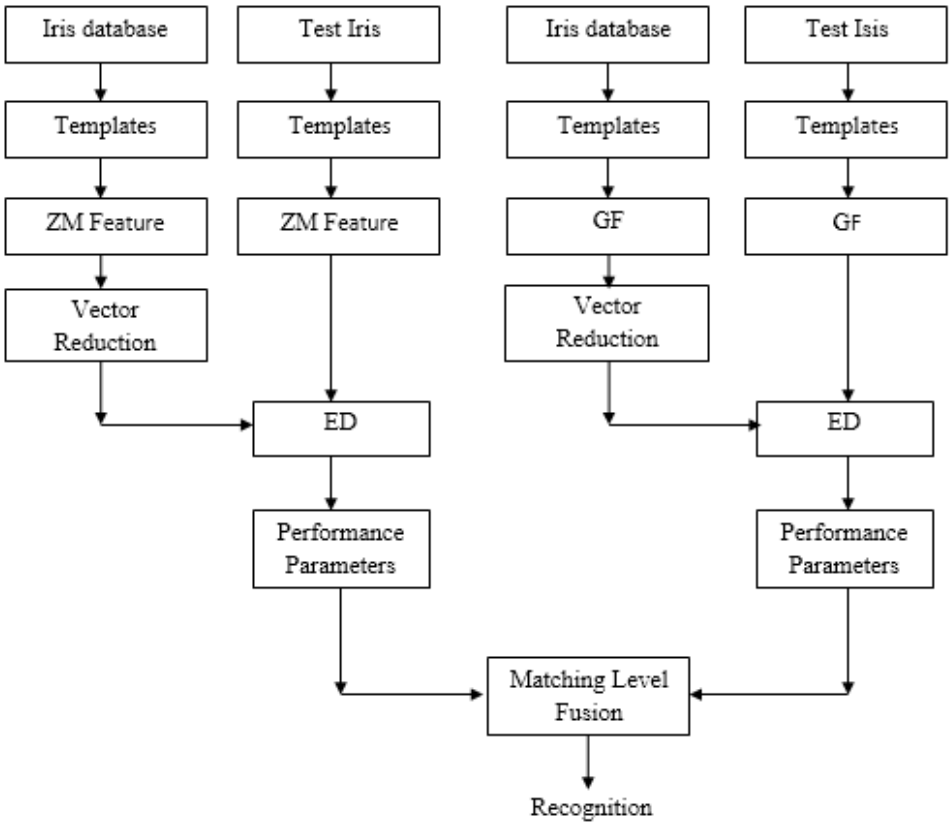

Figure 1. Block diagram of proposed model.

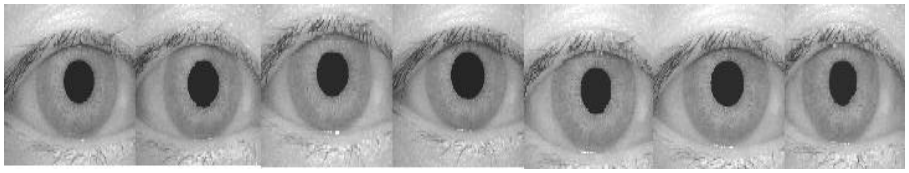

Figure 2. Seven Samples of single person (CASIA V.1 database)

3.2 Iris templates

The iris is the circular portion between inner pupil and outer sclera. The horizontal iris part is considered and extracted for iris template. The vertical iris part ie., above and below the pupil is removed as the little portion is occupied by eyelids and eyelashes. The horizontal iris template is obtained using iris localization and segmentation.

3.2.1 Iris Localization

The black portion in an eye is pupil, hence it has low intensity values. The sclera is brightest portion in an eye, hence the intensity value are high. The circular iris portion has intensity values between pupil and sclera. The appropriate threshold intensity values are fixed and masking upper intensity values to locate pupil as shown in the figure 3(a). The binary image is subjected to connected component analysis, which scans the image and tag the binary image. The maximum diameter of pupil is obtained using equi-diameter region properties of connected component analysis of binary image as shown in figure 3(b).

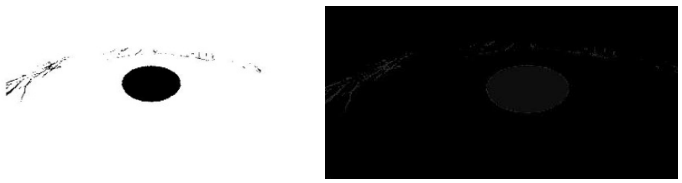

(a) Pupil with eyelashes (b) extracted pupil

Figure 3. Extraction of pupil from an eye image

3.2.2 Iris Segmentation

The iris part is extracted from an eye image using segmentation. The centroid and bounding box are used to local center and radius of localized pupil. The upper and lower portions of pupil are removed by manipulating pupil radius and outer radius of pupil vertically to avoid eyelids and eyelashes in iris part as shown in figure 4(a). The horizontal iris portion nearer to pupil is considered by taking 45 pixels left and right of pupil boundary based on springer CASIA V.1 database analysis [15] as shown in

figure 4(b). The left and right side portions of iris parts are concentrated to obtain iris template.

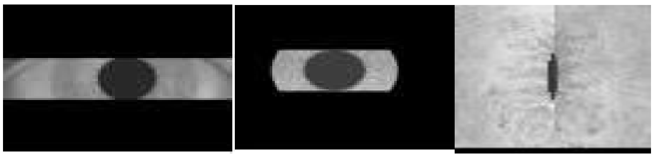

(a)Localized iris part (b) segmented iris (c) Iris Template

Figure 4. Iris Template formations

3.3 Zernike Moments (ZM):

A statistical measure of pixel distribution around centre of gravity of an image which capture global character shaper information. The ZM are designed to capture both global and geometric information of an image. The ZM are invariant to image. The digital image of square size is mapped to the unit circle with its origin at the images center to compute ZM's. The pixels falling outside the unit circle are discarded. The gray-scale image is converted into binary image for ZM. The square image is converted into polar coordinate as shown in Figure 5.

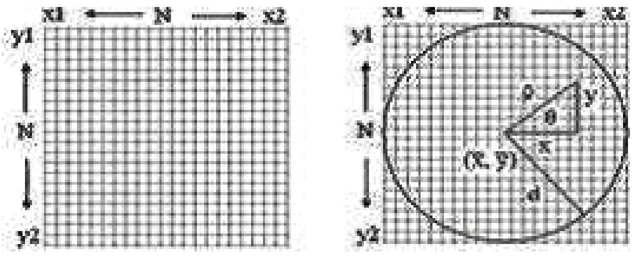

(a) NxN image (b) Unit Circle Mapped image bitmap onto.

Figure 5. Image Conversion

The size of an image is N*N with x1 x2 are x-axis dimension and y1 y2 are y-axis dimensions. The center of the limit disc is (x', y') with is polar value and is polar angle. The image mapped to polar co-ordinate by computing distance *d* as given as equation 1.

$$d = \sqrt{\left(\frac{(x2-x')^2}{2}\right) + \left(\frac{(y2-y')^2}{2}\right)} \ldots\ldots\ldots\ldots\ldots\ldots\ldots\ldots\ldots (1)$$

The distance vector and angle for any pixel (x, y) in polar co-ordinate are computed using equation 2 and 3.

$$\rho = \sqrt{\frac{(x-x')^2+(y-y')^2}{d}} \ldots\ldots (2)$$

$$\theta = tan^{-1}\frac{(x-x')}{(y-y')} \ldots\ldots (3)$$

The Zernike complex polynomials (x, y) which form a complete orthogonal set over the unit disc of $x_2+y_2 \leq 1$ is polar co-ordinate is given in equation 4.

$$V_{ab}(x,y) = V_{ab}(\rho,\theta) = R_{ab}(\rho)e^{jb\theta} \ldots\ldots (4)$$

Where radial polynomial is given equation 5.

$$R_{ab}(\rho) = \sum_{k=0}^{p}(-1)^k \frac{(a-k)!}{k!\,(p-k)!\,(q-k)!} * \rho^{a-2k} \ldots\ldots (5)$$

Where a ≥ 0, |*b*| ≤*a*, *a* - |*b*| = even,

, p = (*a* − |*b*|) /2, q = (*a* + |*b*|) /2

a = order of Zernike moments and non-negative integer.

b = Repetitions and it is an integer that satisfies the conditions.

The ZM of order *a* and repetition *b* is computed using equation 6.

$$Z_{ab} = \frac{a+1}{\pi}\sum\sum I(\rho,\theta)V^*{}_{ab}(\rho,\theta) \ldots\ldots (6)$$

Where *is the complex conjugate. The ZM for order 10 with first 66 moments are given in the table 1.

Table 1. List of Zernike moments up to order *a*=10

a\b	0	1	2	3	4	5	6	7	8	9	10
0	R_{00}	-									
1	-	R_{11}									
2	R_{20}	-	R_{22}								
3	-	R_{31}	-	R_{33}							
4	R_{40}	-	R_{42}	-	R_{44}						

5	-	R_{51}	-	R_{53}	-	R_{55}					
6	R_{60}	-	R_{62}	-	R_{64}	-	R_{66}				
7	-	R_{71}	-	R_{73}	-	R_{75}	-	R_{77}			
8	R_{80}	-	R_{82}	-	R_{84}	-	R_{86}	-	R_{88}		
9	-	R_{91}	-	R_{93}	-	R_{95}	-	R_{97}	-	R_{99}	
10	R_{100}	-	R_{102}	-	R_{104}	-	R_{106}	-	R_{108}	-	R_{1010}

3.4 Gabor Filter

Gabor filters are generally used in texture analysis, edge detection, feature extraction, disparity estimation etc. Gabor filters are special classes of band pass filters, i.e., they allow a certain band of frequencies and reject others. The Gabor filters are useful in extracting the global and local information's of the iris. These are used in texture segmentation, document analysis, edge detection, and image coding and image representation. It offers optimal resolution in space and time domains. It provides better visual representation in the comprised texture images. But the existing parameters require more time consumption for feature extractions. The Gabor filter is the form of sine wave modulated by the Gaussian coefficients as given in equation 7.

$$\psi_{\pi}(f,\theta) = \frac{\cos(2\pi)}{\lambda}(x' + \psi) * e^{-\left(\frac{f^2}{2}x'^2 + \gamma^2 \frac{f^2}{2}y'^2\right)} \ldots\ldots\ldots\ldots\ldots\ldots\ldots\ldots\ldots\ldots\ldots\ldots\ldots\ldots (7)$$

Where,

f = bandwidth

=aspect ratio

=orientation of Gaussian kernel and localized sinusoidal plane

$$\left.\begin{aligned} \psi_{u,v}(x,y) &= \psi_{\pi}(f,\theta) \\ f_u &= \frac{f_{max}}{\sqrt{2}^u} \\ \theta_v &= \frac{v}{8}\pi \end{aligned}\right\} \ldots\ldots\ldots\ldots\ldots\ldots\ldots\ldots\ldots\ldots\ldots\ldots\ldots\ldots (8)$$

gives the Gabor filter of scale u and orientation v-pixel coordination x and y of an iris image. f is the bandwidth of spatial sinusoidal plane with value 2.8, the aspect ratio is 0.3, orientation of the Gaussian kernel is 90 degrees, phase angle is 0 and the wavelength is 3.0.

3.5 Vectors Reduction (VR)

The number of iris vectors of a person is converted into single iris vector per person using averaging technique. The translation of six iris vector images of single person into one iris vector which increases the execution speed and requires less memory

while creating iris vector database. The converting six iris vectors of a single person into one iris vector is as shown in figure 6.

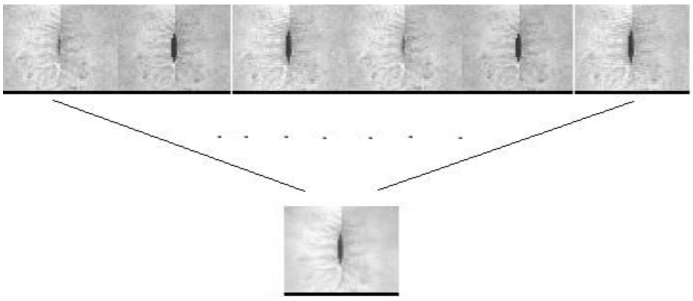

Figure 6. Vectors Reduction from six images to single image

3.6 Euclidean distance

The distance between database features (a_i) and test database (b_i) features is given in equation 9.

$$ED = \sqrt{\sum_{i=1}^{N}(a_i - b_i)} \ldots\ldots (9)$$

Where,

N=Number of coefficients in a vector

= Coefficient values of vectors in the database

= Coefficient values of vectors in the test image

The ED is use to get similarities and dissimilarities of iris images to verify the performance.

3.7 Matching level Fusion

The performance Parameters such as percentage optimum TSR and EER values are fused based score level fusion using normalization technique and is given in equation 10.

$$Normalization\ Fusion = \left[\frac{Actual\ value\ of\ Opt.TSR\ of\ ZM}{Actual\ value\ of\ Opt.TSR\ of\ GF}\right] * [MaxTSR\ of\ GF] \ldots (10)$$

4. PERFORMANCE ANALYSIS

In this section, the definitions of performance parameters are given and also presented experimental results obtained from publicly available database CAISA V.1 to test the performance of the proposed iris recognition method.

4.1 Definitions of Performance Parameters

4.1.1 False Rejection Rate (FRR): It is defined as the probability of genuine persons being rejected as an imposter. It is the ratio of number of genuine persons rejected to the total number of persons inside the database and is computed in equation 11.

$$FRR = \frac{number\ of\ genuine\ persons\ rejected}{total\ number\ of\ persons\ inside\ the\ database} \quad \ldots\ldots\ldots\ldots\ldots\ldots\ldots (11)$$

4.1.2 False Acceptance Rate (FAR): Is defining as the probability of imposter being accepted as genuine persons. It is ratio of imposters accepted as genuine persons from outside the database to the total number of persons in the outside database and is computed in equation 12.

$$FAR = \frac{number\ of\ imposter\ accepted\ as\ genuine\ persons}{total\ number\ of\ persons\ outside\ the\ database} \ldots\ldots\ldots\ldots\ldots\ldots (12)$$

4.1.3 Equal Error Rate (EER): Is defined as error trade of between FRR and FAR i.e., FAR = FRR for a particular threshold value. A lower EER value indicates better performance of biometric systems.

4.1.4 Total Success Rate (TSR): Is the measure of accuracy of biometric systems. It is the ratio of the total number of genuine persons identified correctly in the database to the total number of persons inside the database and is computed in equation 13.

$$TSR = \frac{genuine\ persons\ identified\ correctly}{total\ number\ of\ persons\ inside\ the\ database} \ldots\ldots\ldots\ldots\ldots\ldots\ldots (13)$$

- Optimum Total Success Rate (Opt.TSR): The value of TSR corresponding to the EER for specified threshold.
- Maximum Total Success Rate (Max.TSR): The value of maximum TSR for specified threshold value irrespective of error value.

4.2 Performance variations:

The variations of performance parameter with threshold for different combinations of Person Inside Database (PID) and Person Outside Database (POD) using ZM, GF and proposed fusion techniques are analyzed in this section. The comparison of proposed method using the existing methods is also discussed in this section.

4.2.1 Experimental results using ZM for different combination of PID and POD's:

The variations of performance parameters such as percentage FRR, FAR and TSR with threshold using ZM for different combination of PID and POD's are analyzed in this section. The percentage variations of FAR, FRR and TSR with threshold for PID and POD combination of 20:80, 30:70, 50:50, 60:40 and 80:20 are given in Table 2,3,4,5 and 6 respectively. The percentage FRR value decreases with increasing in threshold values and the value is 100% for lower values of the threshold for all combinations of PID and POD.

The percentage of FAR and TSR increases with threshold values and attains maximum value for higher threshold for all combinations of PID and POD's. The maximum TSR values for all combinations of PID and POD is 100% for higher values of threshold.

The percentage variation of FRR, FAR and TSR are plotted in the figure7,8,9,10 and 11 for PID and POD combinations of 20:80, 30:70, 50:50, 60:40 and 80:20 respectively. It is observed that the percentage FRR values decreases with threshold and the percentage of FAR and TSR are increases with threshold values. The percentage values of FRR and TSR are 100% for the lower and higher values of threshold respectively. The percentage EER values are 16,14,16,15 and 14 for the PID and POD combinations of 20:80, 30:70, 50:50, 60:40 and 80:20 respectively. The EER values are almost constant around 15 for all combination of PID and POD's. The percentage optimum TSR (opt.TSR) are 85, 86.6, 84, 85 and 84for PID and POD combinations of 20:80, 30:70, 50:50, 60:40 and 80:20 respectively.

Table 2. Performance variations with threshold for PID and POD combination of 20 & 80 using ZM technique.

Threshold	%FRR	%FAR	%TSR
0.57	100	0	0
0.58	95	0	5
0.69	35	0	65
0.70	30	3.75	70
0.74	20	12.5	80
0.75	15	17.75	85
0.76	15	18.75	85
0.77	10	23.75	90
0.84	5	72	95
0.85	0	80	100

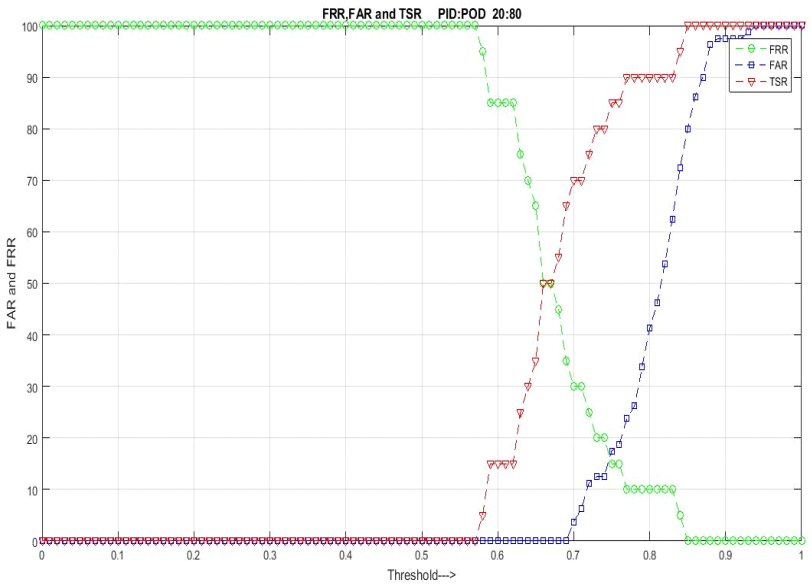

Figure 7. Performance curves using ZM for PID and POD combinations of 20 & 80

Table 3. Performance variations with threshold for PID and POD combination of 30 & 70 using ZM technique.

Threshold	%FRR	%FAR	%TSR
0.54	100	0	0
0.69	36.6	0	63.3
0.70	33.3	2.8	66.6
0.73	23.3	11.4	76.6
0.74	16.6	14.2	83.3
0.75	13.3	14.0	86.6
0.77	13.3	24.5	86.6
0.79	10	30.0	90.0
0.82	3.3	68.5	96.6
0.84	0	75.7	100

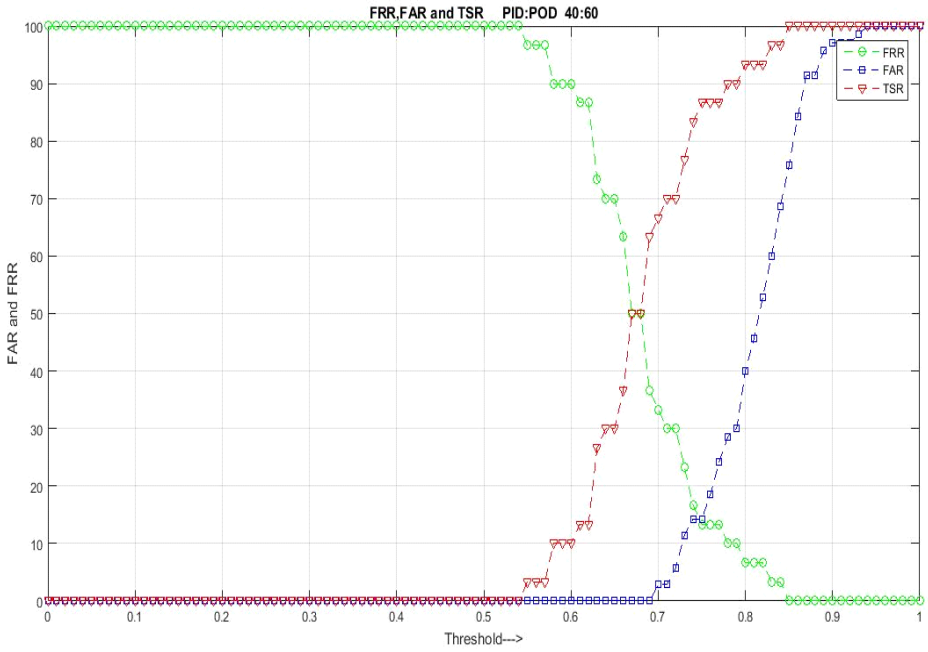

Figure 8. Performance curves using ZM for PID and POD combinations of 30 & 70

Table 4. Performance variations with threshold for PID and POD combination of 50 & 50 using ZM technique.

Threshold	%FRR	%FAR	%TSR
0	100	0	0
.05	100	0	0
0.35	100	0	0
0.50	96.0	0	4.0
0.55	90.0	0	10.0
0.65	50.0	0	50.0
0.70	22.2	4.0	78.0
0.73	16.6	13.6	82.0
0.75	12.2	30.0	88.0
0.90	0	98.0	100

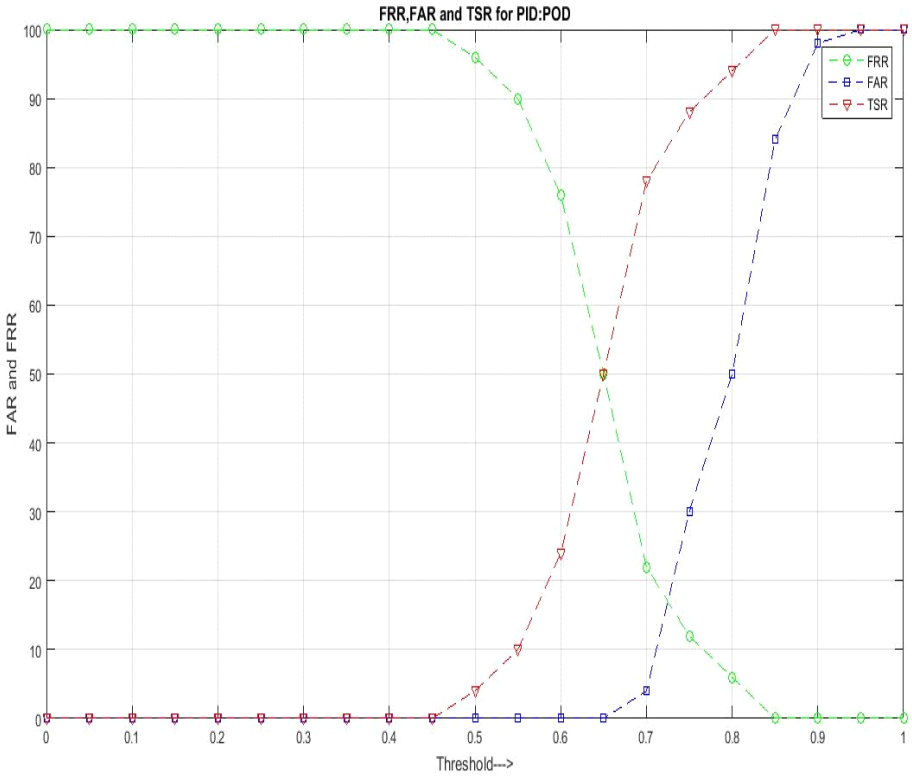

Figure 9. Performance curves using ZM for PID and POD combinations of 50 & 50

Table 5. Performance variations with threshold for PID and POD combination of 60 & 40 using ZM technique.

Threshold	%FRR	%FAR	%TSR
0.56	100	0	0
0.60	68.3	0	31.6
0.69	21.6	0	78.3
0.70	20.0	5.0	80.0
0.73	15.3	15.0	85.0
0.74	13.3	20.0	86.6
0.75	10.0	27.5	90.0
0.81	5.0	60.0	95.0
0.84	1.6	82.5	98.8
0.87	0	90.0	100

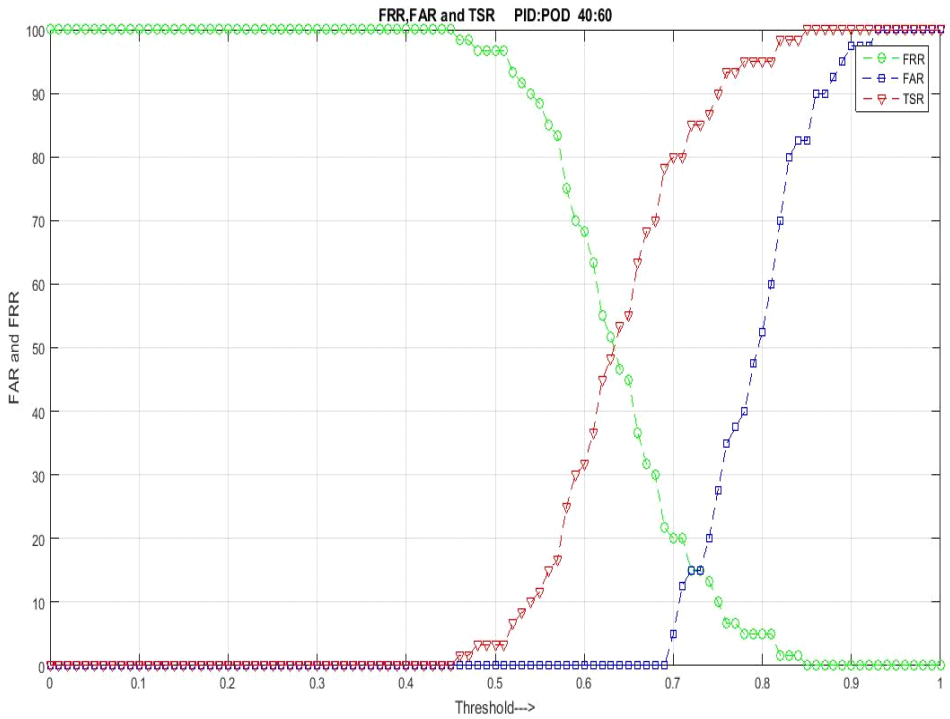

Figure 10. Performance curves using ZM for PID and POD combinations of 60 & 40

Table 6. Variation Performance variations with threshold for PID and POD combination of 80 & 20 using ZM technique.

Threshold	%FRR	%FAR	%TSR
0.52	100	0	0
0.59	67.5	0	32.5
0.68	25.0	10.0	75.0
0.73	16.25	15.0	82.5
0.74	13.75	20.0	85.0
0.76	6.25	35.0	90.0
0.77	3.7	45.0	92.5
0.83	2.5	90.0	92.5
0.87	0	100	95.0
0.90	0	100	100

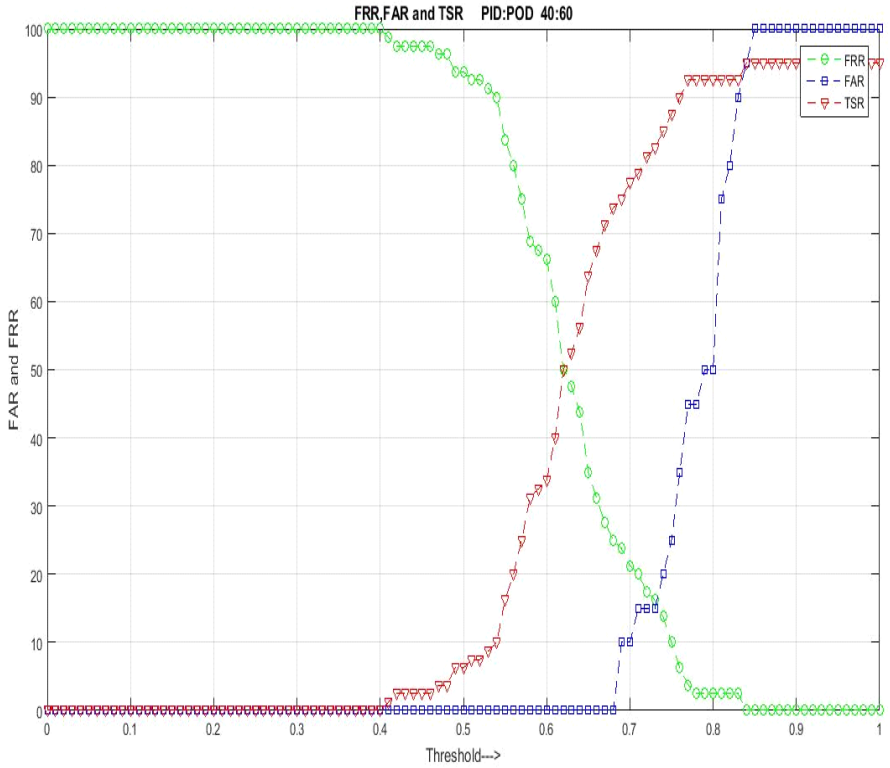

Figure 11. Performance curves using ZM for PID and POD combinations of 80 & 20

4.2.2 Experimental results using GF for different combinations of PID and POD's

The performance parameter such as percentage FRR, FAR, TSR and EER and their variations with threshold values for different combinations of PID and POD's are discussed in this section. The variations of performance parameters with threshold for different PID and POD combinations of 20:80, 30:70, 50:50, 60:40 and 80:20 are given in table 7,8,9,10 and 11 respectively.

The values of percentage FAR and TSR increases with increase in threshold values. The maximum percentage TSR is 100 for all combinations of PID and POD's for higher values of threshold. The percentage value of FRR is zero for higher values of threshold and FAR value is zero for low values of threshold. The graphical representation of percentage FRR, FAR and TSR for variations of threshold values are given in Figure 12,13,14,15 and 16 for different combinations of PID and POD's. It is observed that the percentage FRR and FAR values decrease with increase in threshold values. The percentage values of TSR and FAR increases in increases in threshold values. The percentage EER values are 14,10,18,14 and 15 for the PID and POD combinations of 20:80, 30:70, 50:50, 60:40 and 80:20 respectively. The percentage optimum TSR values are 85,90,82,85 and 85 for PID and POD

combinations of 20:80, 30:70, 50:50, 60:40 and 80:20 respectively. The maximum percentage TSR value is 100 for all combinations of PID and POD.

Table 7. Performance variations with threshold for PID and POD combination of 50 & 50 using GF technique.

Threshold	%FRR	%FAR	%TSR
0.54	100	0	0
0.55	95	0	4
0.68	40	0	60
0.69	30	1.25	70
0.73	20	10	80
0.75	15	13.75	85
0.76	15	17.75	85
0.80	10	38.75	90
0.84	5	66.25	95
0.85	0	76.6	100

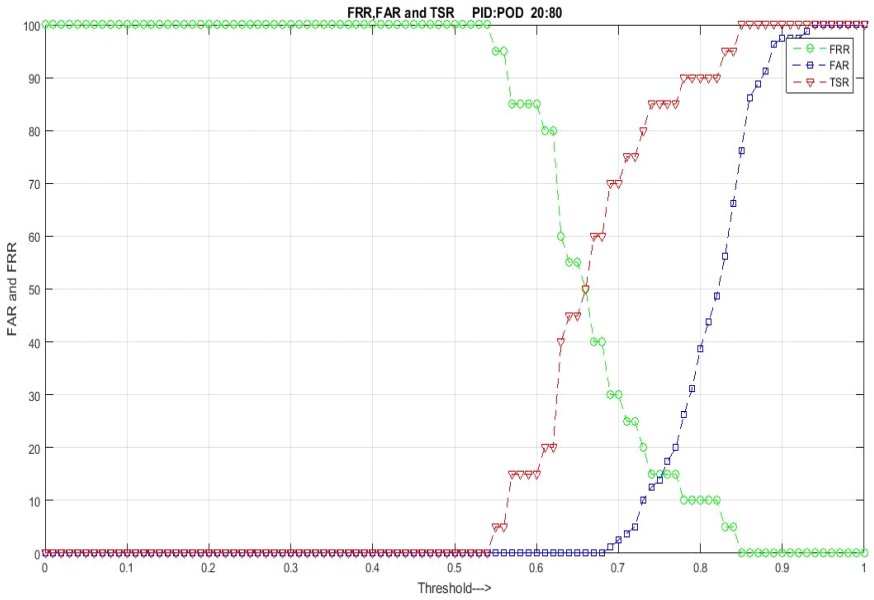

Figure 12. Performance curves using GF for PID and POD combinations of 20 & 80

Table 8. Performance variations with threshold for PID and POD combination of 30 & 70 using GF technique.

Threshold	%FRR	%FAR	%TSR
0.54	100	0	0
0.66	36.6	0	63.3
0.69	26.6	2.8	73.3
0.71	20	7.1	80.0
0.72	16.6	8.5	83.33
0.73	10	11	90.00
0.74	6.6	12.8	93.3
0.75	6.6	18.5	93.3
0.78	3.3	30.0	96.66
0.93	0	97.5	100

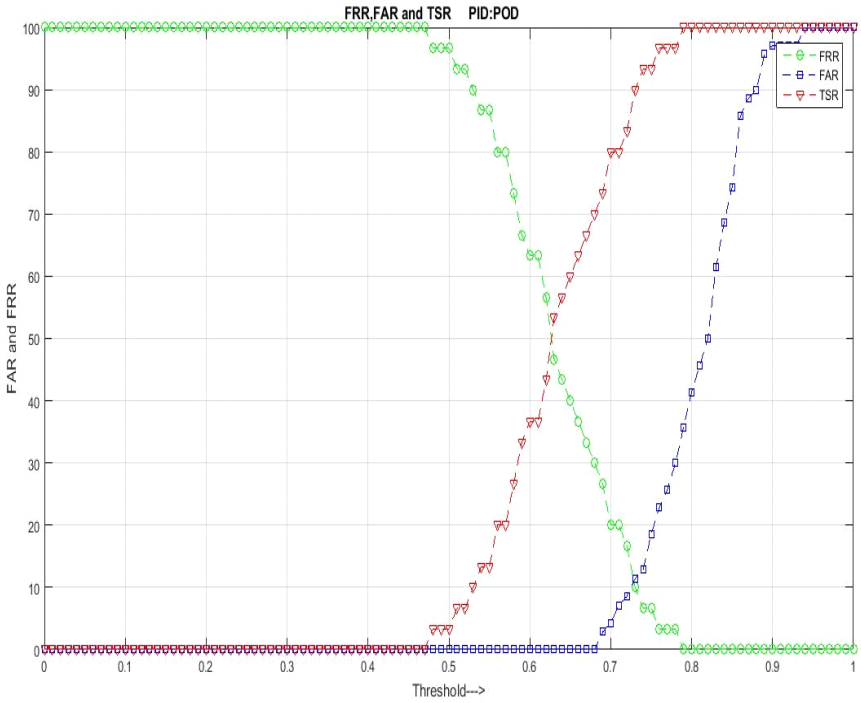

Figure 13. Performance curves using GF for PID and POD combinations of 30 & 70

Table 9. Performance variations with threshold for PID and POD combination of 50 & 50 using GF technique.

Threshold	%FRR	%FAR	%TSR
0.50	100	0	0
0.64	52.0	0	48.0
0.69	24.0	2.0	76.0
0.71	22.0	12.0	78.0
0.72	18.0	16.0	82.0
0.73	18.0	16.0	82.0
0.75	10.0	30.0	90.0
0.77	8.0	36.0	92.0
0.81	6.0	58.0	94.0
0.92	0	98	100

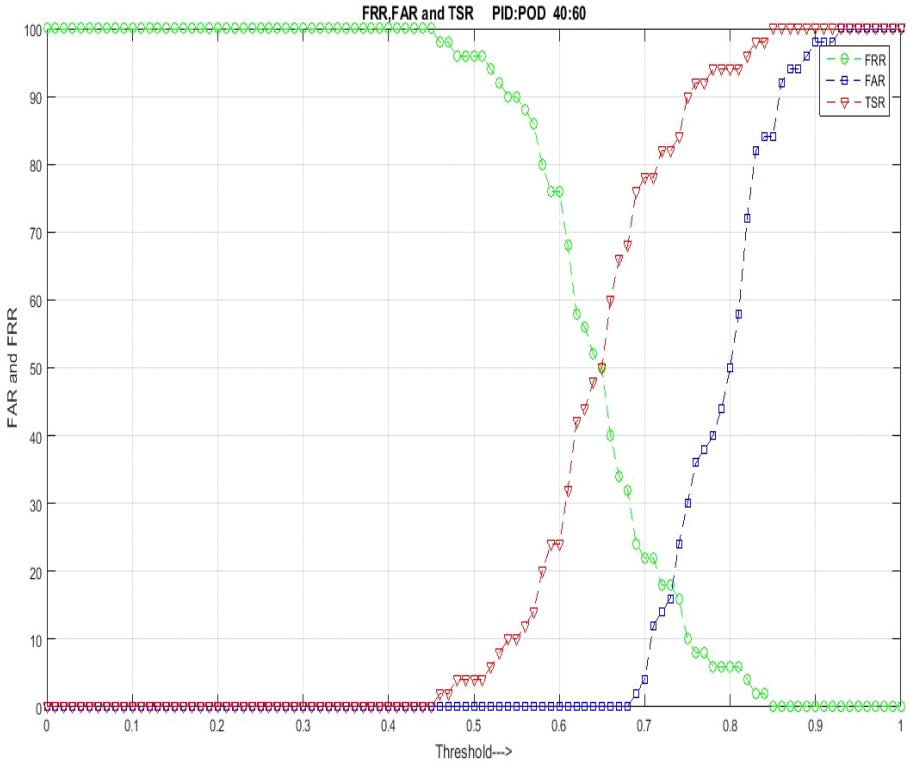

Figure 14. Performance curves using GF for PID and POD combinations of 50 & 50

Table 10. Performance variations with threshold for PID and POD combination of 60 & 40 using GF technique.

Threshold	%FRR	%FAR	%TSR
0.44	100	0	0
0.62	53.3	0	46.6
0.68	30	0	70.0
0.69	21.6	2.5	78.3
0.71	20.0	12.5	80.0
0.72	15.0	15.0	85.0
0.75	8.3	27.5	91.6
0.81	5.0	42.5	95.0
0.84	1.6	82.5	98.33
0.9	0	97.5	100

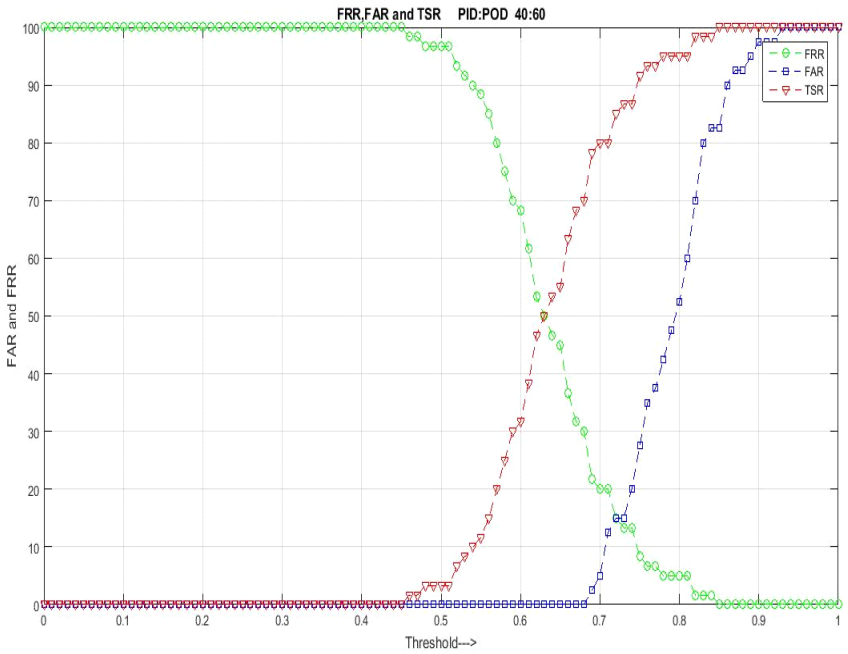

Figure 15. Performance curves using GF for PID and POD combinations of 60 & 40

Table 11. Performance variations with threshold for PID and POD combination of 80 & 20 using GF technique.

Threshold	%FRR	%FAR	%TSR
0.48	100	0	0
0.62	48.75	0	51.2
0.68	23.7	5.0	76.2
0.71	20.0	10.0	78.7
0.73	15.0	15.0	85.0
0.74	12.5	20.0	87.5
0.75	10.0	25.0	90.0
0.78	3.75	45.0	95.0
0.81	2.5	70.0	96.2
0.89	0	100	98.7

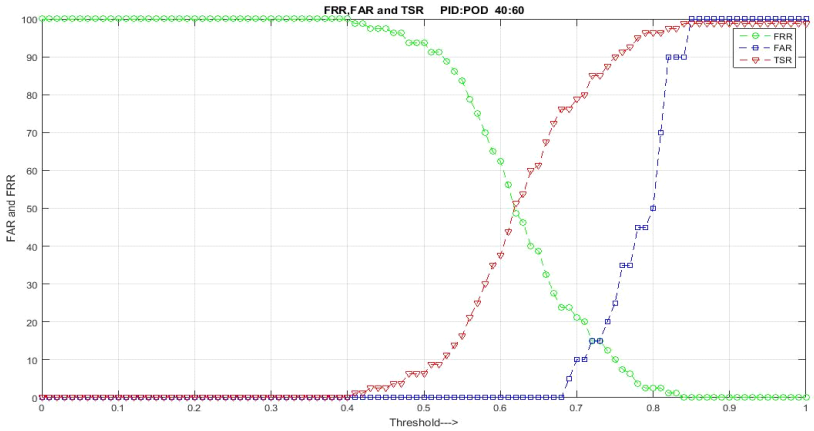

Figure 16. Performance curves using GF for PID and POD combinations of 80 & 20

4.2.3 Experimental results of proposed fusion technique and compared with ZM and GF techniques.

The Performance parameter such as percentage optimum TSR and EER values of ZM and GF techniques are fused at matching level in the proposed model to obtained better performance results. The percentage Opt.TSR and EER values for different combination of PID and POD's with ZM, GF and Proposed fusion techniques are given in Table 12.

Table 12. Comparison of Different Technique with ZM & GF Techniques

PID:POD	ZM		GF		FUSION	
	% Opt.TSR	%EER	% Opt.TSR	%EER	% Opt.TSR	%EER
20:80	85.0	0.16	85	0.14	90.0	11(0.11)
30:70	86.5	0.14	90	0.10	86.5	14(0.14)
50:50	84.0	0.16	82	0.17	93.0	08(0.08)
60:40	85.0	0.15	85	0.14	90.0	10(0.10)
80:20	84.0	0.15	85	0.15	89.0	10(0.10)

4.2.4 Performance comparison of proposed method with existing methods

In order to evaluate the efficiency of our method, we compared it with the existing method in terms of maximum TSR for CASIA iris database. The maximum TSR value of proposed method is 100%, which is better compared to 92.9% and 84.3% values presented by Chun Wei Tan and Ajay Kumar [16] and Rizal Isnonto[17].

Table 13. Performance comparison of proposed method with existing methods.

Sl No.	Author	Techniques	%Max TSR
1	Chun-Wei Tan and Ajay Kumar [16]	Log Gabor +Geo-key Transformation	92.9
2	R. Rizal Isnanto [17]	Bi orthogonal wavelet transform	84.3
3	Proposed Method	Fusion of ZM and GF	100

5. CONCLUSION:

The iris is physiological biometric trait and has unique features even for twins. In this paper, we proposed iris recognition system based on ZM, GF, VR and fusion of performance parameter at matching level. The ROI of iris is obtained using segmentation. The ZM and GF are used to extract feature from ROI of iris. The number of feature vectors of single person are converted into single vector using averaging technique ie., Vector Reduction(VR) to reduce memory and improve the speed of matching. The performance parameters computed from ZM and GF are fused at matching level to improve the performance of biometric system. It is observed that the performance of the proposed method is better compared to existing methods.

REFERENCES:

[1] Mohammed A M Abdullah, Satnam S Dlay, Wai L Woo and Jonathon A Chambers, "Robust Iris Segmentation Method Based on a New Active Contour Force with a Noncircular Normalisation" *IEEE Transactions on systems, Man and Cybernetics: Systems*, pp.1-14, 2016.

[2] John Daugman and Cathryn Downing, "Effect of Severe Image Compressin on Iris Recogntion Performance" *IEEE Transactions on Information Forensics and Security*, Vol. 3, No.1, pp.52–61, March, 2008.

[3] Pattabhi Ramaiah Nalla and Ajay Kumar, "Toward More Accurate Iris Recognition Using Cross-Spectral Matching" *IEEE transactions on Image processing*, Vol.26, No.1, pp.208-221, January, 2017.

[4] Mohd Tariq Khan, Deepak Arora and Shashwat Shukla, "Feature Extraction through Iris Images using 1-D Gabor Filter on Different Iris Datasets" *IEEE International Conferenceon contemporary computing (IC3)*, pp.445-450, 2013.

[5] Chun-Wei Tan and Ajay Kumar "Efficient Iris Segmentation using Grow-Cut Algorithm for Remotely Acquired Iris Images" *IEEE International Conference on biometrics: Theory, Application and System (BTAS*, pp.99-104, 2012.

[6] Hau Ngo, Jennifer Shafer, Robert Ives, Ryan Rakvic and Randy Broussard "Real Time Iris Segmentation on FPGA" *IEEE International Conference on Applications-Specific Systems*, pp.1-7, 2012.

[7] Vaibhav V Dakre and Pravin G Gawande "An Efficient Technique of Multimodal Biometrics using fusion of Face and Iris features" *IEEE International Conference on Advances in Signal Processing*, pp.231-236, June, 2016.

[8] Lydia Elizabeeth B, Duraipandi C, Anju Pratap and Rhymend Uthariaraj V "A Grid based Iris Biometric Watermarking using Wavelet Transform" *International Conference on Recent Trends in Information Technology*, pp.978-989, 2014.

[9] Simina Emerich, Raul Malutan, Eugen Lupu and Laszlo Lefkovits "Patch based Descriptors for Iris Recognition" *IEEE International Conference on Intelligent Computer Communication and Processing (ICCP)*, pp.187-191, 2016.

[10] Diego Gragnaniello, Giovanni Poggi, Carlo Sansone and Luisa Verdoliva "An Investigation of Local Descriptors for Biometric Spoofing Detection" *IEEE transactions on Information Forensics and Security*, Vol. 10, No.4, pp.849–863, April, 2015.

[11] Hau T Ngo, Ryan N Rakvic, Randy P Broussard and Robert W Ives "Resource-Aware Architecture Design and Implementation of Hough

Transform for a Real-Time Iris Boundary Detection System" *IEEE transactions on Consumer Electronics*, Vol.60, No.3, pp.485–492, August, 2014.

[12] Sheng-Hsun Hsieh, Yung-Hui Li, Chung-Hao Tien and Chin-Chen Chang, "Extending the Capture Volume of an Iris Recognition System using Wavefront Coding and Super-Resolution" *IEEE Transactions on Cybernetics*, Vol.46, No.12, pp.3342-3350, December, 2016.

[13] R Raghavendra and Christroph Busch "Robust Scheme for Iris Representation Attack Detection Using Multiscale Binarized Statistical Image Features" *IEEE Transactions on Information Forensics and Security*, Vol. 10, No.4, pp.703–715, April, 2015.

[14] Nadia Othman and Bernadette Dorizzi "Impact of Quality-Based Fusion Techniques for Video-Based Iris Recognition at a Distance" *IEEE transactions on Information Forensics and Security*, Vol. 10, No.8, pp.1590–1602, August 2015.

[15] http://www.sinobiometrics.com, CASIA Iris Image Database.

[16] Chun-Wei Tan and Ajay Kumar "Efficient and Accurate At-a-Distance Iris *Recognition* Using Geometric Key-Based Iris Encoding" *IEEE Transaction on Information Forensics and Security*, Vol. 9, No. 9, pp-1518-1526, September 2014.

[17] R. Rizal Isnanto "Isis Recognition Analysis Using Biorthogonal Wavelets Transform for Feature Extraction" *IEEE International conference on Information Technology, Computer and Electrical Engineering*, pp.183-187, March 2015.